Proc. Nat. Acad. Sci. USA
Vol. 70, No. 11, pp. 3255–3259, November 1973

Patterns of Spatiotemporal Organization in an Allosteric Enzyme Model

(irreversible thermodynamics/dissipative structures/chemical waves/glycolytic oscillations)

A. GOLDBETER*

Faculté des Sciences, Université Libre de Bruxelles, Brussels, Belgium

Communicated by I. Prigogine, July 3, 1973

ABSTRACT **The behavior of a model for an allosteric enzyme oscillator activated by the reaction product is analyzed in the presence of diffusion. When the concentrations of the chemicals are fixed at the boundaries, dynamic dissipative structures are shown to arise in the form of propagating concentration waves. The model is applied to the phosphofructokinase reaction and suggests that a spatiotemporal organization may originate at a macroscopic (supracellular) level from the glycolytic system.**

Glycolytic oscillations observed in yeast cells (1) and in cell-free extracts of yeast (2, 3) and muscle (4) originate from the positive feedback exerted on phosphofrucktokinase by one of the products of the enzymatic reaction (1–4). Several models based on this property have been proposed for glycolytic periodicities (5, 6). Taking explicitly into account the cooperative kinetics of phosphofrucktokinase (3, 7, 8), Lefever and I have recently analyzed a model for an allosteric enzyme activated by the reaction product (9). The limit cycle behavior of this model compares with glycolytic oscillations observed in yeast extracts (9, 10).

Additional patterns of dynamic behavior are allowed by diffusion (11). In particular, the existence of chemical waves has been reported in a theoretical analysis of a model (12, 13) and in experiments on the Belousov–Zhabotinsky reaction (14, 15). The object of this communication is to determine how diffusion and boundary constraints may induce the formation of such a spatiotemporal organization in the allosteric model.

With the periodic boundary conditions† considered earlier (9), the stability analysis of the homogeneous steady state shows that even when this state is unstable with respect to inhomogeneous perturbations the system undergoes a spatially uniform stable limit cycle. Thus the effect of diffusion does not lead to any space-dependent structure under these conditions. In this paper, I show that concentration waves may arise in the system when the periodic boundary conditions are replaced by the assumption that the concentrations of the chemicals are maintained constant at the boundaries.

I briefly recall in section 1 the general features of the model and some results concerning the limit cycle oscillations. In section 2, I deal with the occurrence of propagating waves and other types of space-dependent regimes. Section 3 is devoted to a discussion of these results.

* Present address: Polymer Department, Weizmann Institute of Science, Rehovot, Israel.

† These conditions impose that the value of a dependent variable X at a point r satisfies: $X(r) = X(r + L)$ where L is a characteristic dimension of the system.

1. Sustained oscillations in the allosteric model

As a detailed presentation of the model has appeared elsewhere (9), I summarize the main assumptions and give the final kinetic equations of the system.

Structural Hypotheses. We consider a monosubstrate allosteric enzyme consisting of two protomers. Each protomer may exist under two conformations: active (R) and inactive (T). The transition between these two conformations is fully concerted (16). The substrate binds to the R and T forms with different affinities but only the R complexes decompose to yield the product; the latter binds exclusively to the active form and is therefore a positive effector of the enzyme.

Environmental Hypotheses. The substrate is supplied at a constant rate and the product is removed by a monomolecular reaction.

Assuming a quasi-steady-state hypothesis for the enzymatic forms, the evolution of the metabolite concentrations in time and space is given by the equations

$$\frac{\partial \alpha}{\partial t} = a\left[\sigma_1 - \frac{\left(\frac{2D_0\epsilon}{\epsilon+1}\right)\alpha\left(1+\frac{\alpha}{\epsilon+1}\right)(1+\gamma)^2}{\mathcal{L}(1+\alpha c)^2 + (1+\gamma)^2\left(1+\frac{\alpha}{\epsilon+1}\right)^2}\right] + \mathcal{D}_\alpha \frac{\partial^2 \alpha}{\partial r^2} \quad [1a]$$

$$\frac{\partial \gamma}{\partial t} = a\left[\frac{\left(\frac{2D_0\epsilon}{\epsilon+1}\right)\alpha\left(1+\frac{\alpha}{\epsilon+1}\right)(1+\gamma)^2}{\mathcal{L}(1+\alpha c)^2 + (1+\gamma)^2\left(1+\frac{\alpha}{\epsilon+1}\right)^2} - \sigma_2\gamma\right] + \mathcal{D}_\gamma \frac{\partial^2 \gamma}{\partial r^2} \quad [1b]$$

where α and γ denote, respectively, the concentrations of the substrate (S) and the product (P)‡ divided through the dissociation constants of the enzyme complexes (16) $K_{S(R)} = K_{P(R)} = d/a$; D_0 is the total enzyme concentration; σ_1 is the reduced injection rate of the substrate; ϵ and σ_2 are, respectively, related to the irreversible decomposition of the active enzyme–substrate complexes and to the outflow of the product; $\mathcal{L}$ is the allosteric constant; c is the nonexclusive binding coefficient for the substrate; and $\mathcal{D}_\alpha$ and $\mathcal{D}_\gamma$ are the

‡ In the glycolytic example, α and γ refer to ATP and ADP, respectively (9).

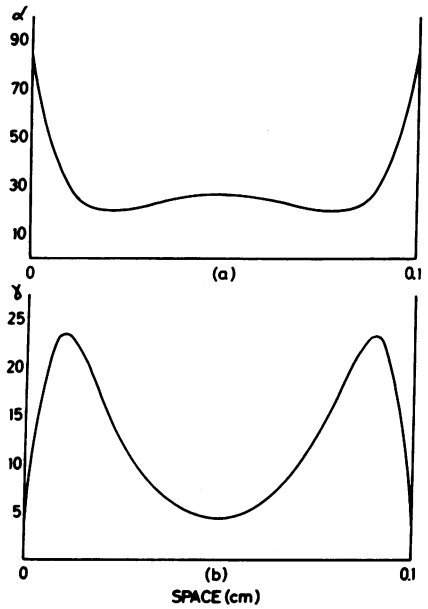

FIG. 1. Spatial distributions of the substrate (a) and product (b) normalized concentrations for $D_0 = 5 \times 10^{-4}$ mM, $a = 10^5$/mM·sec, $\epsilon = 10^{-1}$, $c = 10^{-2}$, $\mathcal{L} = 5 \times 10^6$, $\sigma_1 = 5\sigma_2 = 5 \times 10^{-7}$ mM, $K_{S(R)} = K_{P(R)} = 5 \times 10^{-2}$ mM, and $\mathfrak{D}_\alpha = \mathfrak{D}_\gamma = 10^{-6}$ cm²/sec. The dimension of the system is 0.1 cm. The values $\alpha = 84.285$ and $\gamma = 3.284$ are maintained at the points 1 and M; they correspond to the maximum substrate concentration on the homogeneous limit cycle (see Fig. 3).

diffusion coefficients of the substrate and the product, respectively. Transport by diffusion along a single dimension is considered to be effective for the metabolites only.

When diffusion is neglected, the set of equations [**1a**, **1b**] admits one physically acceptable steady state. The conditions for which this homogeneous state becomes an unstable focus or node were determined by normal mode analysis. Numerical integration confirms that the unstable point is enclosed in the (α–γ) phase plane by a limit cycle which corresponds to sustained oscillations of the substrate and product concentrations in time (9). From a thermodynamic point of view, this limit cycle represents a temporal *dissipative structure*, i.e., a time-coherent state appearing in an abrupt way beyond a nonequilibrium instability (11; 17, 18). The thermodynamic requirement that the limit cycle behavior only arises in open systems operating far from equilibrium is certainly satisfied: the source of the substrate, the sink of the product, and the decomposition of the R complexes being completely irreversible, the system functions at an infinite distance from equilibrium.

A point directly accessible to experiments concerns the effect of varying the substrate injection rate. The system undergoes sustained oscillations in a finite interval of σ_1 values ($1.05\sigma_2 \leqslant \sigma_1 \leqslant 13\sigma_2$ for the set of parameters of Figs. 1 and 2 below, in the homogeneous limit where diffusion is neglected) and remains stable outside this domain, although enzyme saturation may occur for large injection rates. As the system crosses the unstable region, the amplitude of the oscillations goes through a maximum whereas the period decreases (10). These results are in agreement with the observations of Hess *et al.* on yeast extracts (3).

2. Patterns of spatiotemporal organization

Let us consider the effect of diffusion in a unidimensional system. When the concentrations of the chemicals are fixed at the boundaries (Dirichlet conditions), various types of space-dependent structures arise depending on the dimension of the system, the diffusion coefficients, and the boundary values of α and γ. These solutions may be classified as time-independent regimes, standing waves, and propagating waves. It will turn out that the domain of parameters giving rise to sustained oscillations in the homogeneous case is the most suitable one for the occurrence of wavelike solutions, since it allows for interferences between temporal periodicities and boundary constraints. In this domain, for given values of the diffusion coefficients and the boundary conditions, different kinds of regime are realized in turn by varying the size of the system.

The simulation study of the allosteric model involves the integration of Eqs. **1a** and **1b** on a digital computer. Consider-

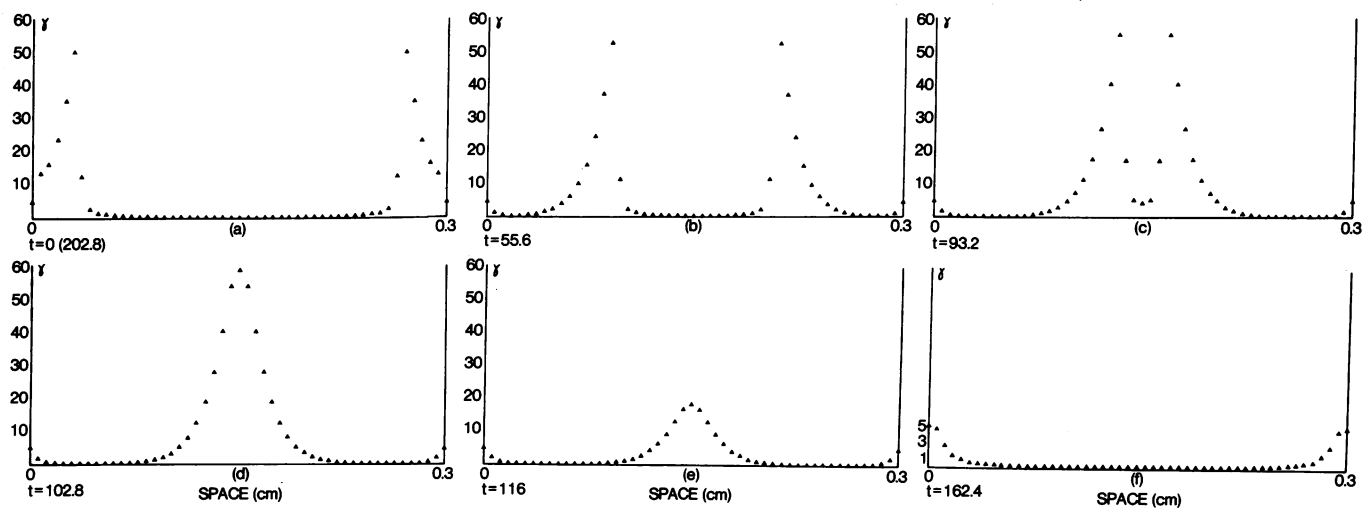

FIG. 2. Distribution of concentration γ as a function of position at successive time intervals on a period ($t = 202.8$ sec). The time is set to zero in (a), some 20 periods after the phenomenon started from the unstable homogeneous steady state. The dimension of the system is 0.3 cm. The steady-state concentrations $\alpha = 40.1986$ and $\gamma = 5$ are maintained at the boundaries. The curves have been established for $D_0 = 5 \times 10^{-3}$ mM, $\sigma_1 = 5\sigma_2 = 5 \times 10^{-6}$ mM, and $M = 51$; other constants are as in Fig. 1.

ing the space as a linear mesh of M equidistant points, I represent diffusion terms in the form of central finite differences and specify the boundary conditions by fixing the concentrations α and γ at the points 1 and M. The resulting system of ordinary differential equations is integrated by the means of a Runge–Kutta method with regulation of the time step.

Time-Independent Regime. When the dimension of the system is reduced below a critical value (see below for a numerical estimate), one obtains for a certain range of boundary concentrations formation of a spatially organized regime that remains stationary in time. This regime seems to be uniquely determined by the boundary conditions, since the same structure is realized starting from various initial conditions. In the "symmetric" case, where equal concentrations are maintained at both boundaries, the structure for the product γ consists of two identical peaks. This kind of regime is achieved when substrate concentrations as large as twice the steady-state value are maintained at the boundaries (Fig. 1). Similar results are obtained when the substrate enters into the system at the boundaries only ($\sigma_1 = 0$). Among other characteristics of this class of solutions, one observes that the amplitude of the peaks for γ increases with the ratio $\mathcal{D}_\alpha/\mathcal{D}_\gamma$ and with the concentration α imposed at the nearest boundary, as shown by simulations for asymmetric constraints.

At first sight, the stationary distributions of Fig. 1 would appear as spatial dissipative structures. Several features suggest, however, that these solutions belong to the *thermodynamic branch* defined by Prigogine as the continuous extrapolation of the situation prevailing near equilibrium (11, 17 18). The observed structures are an effect of the boundary conditions: in the center, the system evolves towards the homogeneous steady state, whereas it reorganizes near the boundaries to take constraints into account, giving rise thereby to a limited number of peaks for the reaction product. Stationary spatial dissipative structures do not depend so strongly on the boundary conditions. Moreover they have a definite wavelength and possess the ability to localize inside the system (11, 12, 17–19).

Standing and Propagating Concentration Waves. Contrary to the stationary regime, spatiotemporal solutions appear beyond a critical point of instability of the thermodynamic branch. For a given dimension, the transition between a time-independent solution and a standing wave is achieved by increasing the diffusion coefficient of the reaction product or lowering the substrate concentration at the boundaries. If the substrate injection rate is chosen to satisfy the homogeneous instability condition, successive extensions of the dimension of the system by one order of magnitude with respect to the time-independent regime or to the standing case give rise first to propagating solutions and then to oscillations remaining quasi-uniform in space.

The main distinction between the two classes of waves concerns the phase difference between successive points in space which corresponds to the appearance of a sharp wavefront in the propagating case. We shall restrict ourselves to the latter situation in view of its biological implications.

The value $\sigma_1 = 5\sigma_2$ in the middle of the limit cycle domain (10) has been chosen for the simulation study. If we impose symmetrically the steady-state values of the concentrations α and γ as boundary conditions, we observe, for definite dimensions of the system, the formation of two sharp wavefronts of the reaction product near the boundaries and their subsequent propagation towards the center where they collide (Figs. 2*a–d*). Then the central peak so formed decreases (Figs. 2*e–f*) until new wavefronts build up at the extremities. This periodic phenomenon is sustained. The spatiotemporal dependence of the substrate is more complex and shall not be considered here.

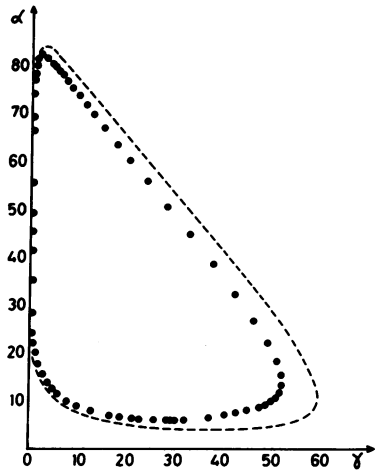

FIG. 3. Limit cycle oscillations at point 15 (*dots*) corresponding to the plateau of the wavefront amplitude, and at the middle point 26 (*dashed lines*) in the case described in Fig. 2.

A detailed examination of the numerical data shows that limit cycle oscillations occur at each point of space with a unique period. The points 4 and 26 (middle point for $M = 51$) are 182° out of phase. All the limit cycles are enclosed by the curve at the middle point which practically coincides with the asymptotic trajectory of the homogeneous case (Fig. 3). This observation suggests that the propagating wave may be considered as resulting from a coupling between several nonlinear oscillators. Starting from the homogeneous steady state, the final oscillatory regime is reached after a stage of synchronization that propagates from the borders of the system and lasts some fifteen periods for $M = 51$.

A comparison of the curves giving the amplitude and the propagation rate of a wavefront as a function of position indicates the existence of three domains. Between points 1 and 8 for $M = 51$, the amplitude of the peak increases whereas it propagates at a constant rate. Beyond point 8 the amplitude reaches a plateau which extends to point 20. This interval is crossed at a constant rate which is slightly less than in the previous domain. Beyond point 21, the wavefront accelerates whereas its amplitude increases, until point 26 approaches the maximum concentration allowed for the homogeneous limit cycle (see Figs. 2 and 3). The calculations performed with 33, 51, and 81 points for a given dimension present few quantitative differences. In the case described in Fig. 2, the plateau values of the amplitude for $M = 33$, 51, and 81 are, respectively, 53.6, 52.2, and 50.8, whereas the propagation rates of the wavefronts in the plateau region are 1.171×10^{-3} cm/sec, 1.068×10^{-3} cm/sec and 1.041×10^{-3} cm/sec. At the same time, the overall period changes from 204 sec to 202.8 sec and 202.4 sec, as compared to the period in the homogeneous case, which is around 213.5 sec.

A gradient in the boundary conditions induces the polarity

of the wave. Maintenance of zero concentrations at one extremity results in unidirectional wavefront propagation towards the sink. In the symmetric case, boundary concentrations for α larger than the steady-state value do not change the behavior of the system qualitatively but lower the plateau level of the amplitude. Periodic phenomena may disappear if the substrate concentration at the boundaries is reduced to some critical value below the steady state.

The effect of the source term σ_1 has also been investigated. Standing waves are observed for finite values of this parameter that do not correspond to limit cycle oscillations. A 10-fold extension of the diffusion space does not result in wave propagation, as the system returns instead to the thermodynamic branch.

As regards the convergence of the numerical integration, we note that the differences observed between calculations performed with various numbers of space intervals are very small. Further evidence for the convergence is seen in time-independent regimes. I have verified the stationary spatial distributions of Fig. 1 by means of a "shooting procedure." At the steady state, Eqs. **1a** and **1b** reduce to a system of four ordinary differential equations of the first order. The initial-value problem is readily solved by noticing that the first derivatives of α and γ with respect to space vanish in the central point of the system for reasons of symmetry. When the initial values of α and γ at this point are taken from the curves of Fig. 1 established for $M = 33$, the latter are recovered by integrating the equations from the central point to one of the boundaries.

3. Discussion

In this paper I have analyzed the interferences between time-periodic solutions and boundary constraints. Below a critical length of the system, diffusion and Dirichlet conditions play an essential role, leading to a stationary spatial configuration on the thermodynamic branch. As the dimension increases, the influence of boundary conditions becomes looser and the solution acquires a spatiotemporal dependence: sustained waves appear, first standing and then propagating into the system. For larger dimensions, the solution becomes quasi-homogeneous in space and tends to the limit cycle observed in the absence of diffusion.

The regimes dominated by diffusion and by the chemical reaction are separated by a critical length of the system, L_c. This parameter, as estimated in *Appendix*, is given by the relation

$$L_c = \left(\frac{8\alpha_0 \mathcal{D}_\alpha}{a\sigma_1}\right)^{1/2} \qquad [2]$$

where α_0 denotes the boundary concentration of the substrate. The dependence of the critical length on the square root of the ratio ($\mathcal{D}_\alpha$/kinetic term) agrees with dimensional analysis and with the simulation study. An interesting feature of Eq. **2** concerns the relation between L_c and the boundary conditions. This point is also verified by computer simulation of the model.

A numerical estimate of space scales for the various structures has been performed for the glycolytic example. Since the intrinsic constants of phosphofructokinase are not known, a choice has been made to match the oscillations observed in yeast extracts with respect to the period and amplitude (see Appendix in ref. 9). This numerical choice has been used to study the effect of diffusion. When the values of the parameters for which an agreement is obtained with respect to limit cycle periodicities are inserted in the model, one finds that the dimensions over which space-dependent structures arise are supracellular and vary between 10^{-2} and 1 cm for the wavelike solutions. Although the equation derived for L_c is a simple estimate, it yields good agreement with the simulation results. For the parameters used in Figs. 1 and 2, relation **2** gives critical lengths of the order of 1.2×10^{-1} cm and 2.5×10^{-2} cm, respectively; a time-independent regime is achieved accordingly for $L = 10^{-1}$ cm in Fig. 1, whereas propagating waves are observed for $L = 0.3$ cm in Fig. 2.

When the significance of the chemical waves is considered, it is interesting to compare the time scale of the phenomenon to the effect of simple diffusion. In the plateau region for the amplitude, the rate of propagation of the wavefront is about 10^{-3} cm/sec in the case described in Fig. 2, when the period of the limit cycle lies in the range of some minutes. The time required by the wavefront to travel at a constant rate over a distance of 6×10^{-2} cm in this region (i.e., 10 intervals in Fig. 2) is about 1 min. In contrast, the time required by the wavefront to spread over a similar distance by diffusion alone is about $(6 \times 10^{-2}\ \text{cm})^2/(10^{-6}\ \text{cm}^2/\text{sec})$, i.e., 1 hr (see also ref. 20). Thus cellular metabolism provides a means of fast transmission of a chemical signal, in the form of a sharp concentration wavefront, over macroscopic distances.

The analysis of the model has been developed for soluble enzyme oscillators only. This situation could be extended to a linear set of cells, assuming that the cell membrane is permeable to the chemical reactants. Under these conditions, the model indicates that a propagating wave may arise from the coupling of several neighboring cells possessing enzyme oscillators synchronized by the source of the substrate. The cells at the extremities of the array have to remain in a steady state with respect to the metabolites involved in the oscillatory mechanism. It follows that patterns of enzyme regulation that give rise to limit cycle periodicities also provide mechanisms for establishing a spatial coherent behavior at the supracellular level.

Space-dependent periodicities of this kind could play some role in embryonic development, as suggested by Goodwin and Cohen (21), since the dimensions for which they arise are those of morphogenetic fields (22, 23). We must note however, that the time scale for the specification of positional information has been shown in many cases to be compatible with a mechanism based on simple diffusion (20).

Experimentally, a wave of cyclic AMP triggers the aggregation of certain species of slime molds (23). According to Cohen and Robertson, this phenomenon appears as the relaying of a chemical pulse due to a cellular periodicity (see ref. 13) by proximate amebas (21, 23). A similar qualitative result is achieved in the allosteric model, where the wavelike solutions result from the concerted behavior of several synchronized oscillators.

Finally, a direct prediction of the model concerns the glycolytic system. The results of this study indicate that spatiotemporal dissipative structures might be observed in the phosphofructokinase reaction over macroscopic dimensions. Such a possibility could be tested on yeast extracts, under suitable interferences between the boundary constraints and the limit cycle regime. Preliminary steps have already been undertaken in this direction (13).

Appendix

An approximate expression for the critical length L_c is obtained easily at the steady state. Since the sign of the derivative $\partial\alpha/\partial t$ changes on the limit cycle, the source term $a\sigma_1$ in Eq. 1a is of the order of the nonlinear contribution from the enzymatic reaction. Since the kinetic term is of the order of $a\sigma_1$, one is left with the approximate relation

$$(d^2\alpha)/(dr^2) = -(a\sigma_1)/\mathfrak{D}_\alpha \qquad [A.1]$$

subject to the boundary conditions $\alpha = \alpha_0$ in $r = 0$ and $r = L$. The solution

$$\alpha(r) = -\left(\frac{a\sigma_1}{2\mathfrak{D}_\alpha}\right) r^2 + \left(\frac{a\sigma_1 L}{2\mathfrak{D}_\alpha}\right) r + \alpha_0 \qquad [A.2]$$

passes through a maximum α_M at $r = L/2$, where the following relation holds:

$$\alpha_M/\alpha_0 = 1 + (a\sigma_1 L^2)/(8\alpha_0\mathfrak{D}_\alpha) \qquad [A.3]$$

The ratio α_M/α_0 gives a measure of the relative importance of chemical reaction and diffusion: the distribution $\alpha(r)$ is uniform for infinite diffusion and becomes parabolic as the kinetic contribution increases. If the critical length is defined as that for which the two terms in the right-hand side of [A.3] are of the same order, one obtains the expression

$$L_c = \left(\frac{8\alpha\mathfrak{D}_\alpha}{a\sigma_1}\right)^{1/2} \qquad [A.4]$$

I thank Prof. I. Prigogine for his continuous interest. I gratefully acknowledge that a first stage of this investigation was done in collaboration with Dr. R. Lefever. I further thank Prof. G. Nicolis for stimulating discussions and Drs. M. Herschkowitz-Kaufman and M. Baus for their suggestions. A.G. is an aspirant du Fonds National Belge de la Recherche Scientifique.

1. Ghosh, A. & Chance, B. (1964) *Biochem. Biophys. Res. Commun.* **16**, 174–181.
2. Hess, B. & Boiteux, A. (1968) in *Regulatory Functions of Biological Membranes*, ed. Järnefelt, J. (Elsevier Publ. Co., Amsterdam-London-New York), pp. 148–162.
3. Hess, B., Boiteux, A. & Krüger, J. (1969) *Advan. Enzyme Regul.* **7**, 149–167.
4. Frenkel, R. (1968) *Arch. Biochem. Biophys.* **125**, 151–156.
5. Higgins, J. (1964) *Proc. Nat. Acad. Sci. USA* **51**, 989–994.
6. Sel'kov, E. E. (1968) *Eur. J. Biochem.* **4**, 79–86.
7. Blangy, D., Buc, H. & Monod, J. (1968) *J. Mol. Biol.* **31**, 13–35.
8. Mansour, T. E. (1972) in *Current Topics in Cellular Regulation*, eds. Horecker, B. L. & Stadtman, E. R. (Academic Press, New York and London), Vol. 5, pp. 1–46.
9. Goldbeter, A. & Lefever, R. (1972) *Biophys. J.* **12**, 1302–1315.
10. Goldbeter, A. & Lefever, R. (1972) in *Analysis and Simulation of Biochemical Systems*, eds. Hemker, H. C. & Hess, B. (North-Holland Publ. Co., Amsterdam), pp. 163–168.
11. Prigogine, I. & Nicolis, G. (1971) *Quart. Rev. Biophys.* **4**, 107–148.
12. Herschkowitz-Kaufman, M. & Nicolis, G. (1972) *J. Chem. Phys.* **56**, 1890–1895.
13. Hess, B., Boiteux, A., Busse, H. G. & Gerisch, G. (1973) "Proceedings of the Workshop Membranes, Dissipative Structures and Evolution" (Brussels, November 1972) *Advan. Chem. Phys.*, in press.
14. Zaikin, A. N., & Zhabotinsky, A. M. (1970) *Nature* **225**, 535–537.
15. Winfree, A. T. (1972) *Science* **175**, 634–636.
16. Monod, J., Wyman, J. & Changeux, J. P. (1965) *J. Mol. Biol.* **12**, 88–118.
17. Glansdorff, P. & Prigogine, I. (1971) *Thermodynamic Theory of Structure, Stability and Fluctuations* (Wiley-Interscience, New York).
18. Nicolis, G. (1971) *Advan. Chem. Phys.* **19**, 209–324.
19. Lefever, R. (1968) *J. Chem. Phys.* **49**, 4977–4978.
20. Crick, F. (1970) *Nature* **225**, 420–422.
21. Goodwin, B. C. & Cohen, M. H. (1969) *J. Theor. Biol.* **25**, 49–107.
22. Wolpert, L. (1969) *J. Theor. Biol.* **25**, 1–47.
23. Robertson, A. & Cohen, M. H. (1972) *Annu. Rev. Biophys. Bioeng.* **1**, 409–464.